Stiff-Glass Approximation of Mode-Coupling Theory

Th. Voigtmann

Physik-Department, Technische Universität München, 85747 Garching, Germany

(Dated: February 1, 2008)

The stiff-glass approximation of the mode-coupling theory of the glass-transition—as introduced in a recent paper by Götze and Mayr for a discussion of phenomena resembling the Boson Peak and High-Frequency Sound observations made in real glass-formers—is examined in detail. It amounts to a neglection of two-phonon processes and thus provides a clear physical picture for the MCT solutions deep in the glass. In addition, the effect of additional symplifying approximations and the combination of these approximations is studied.

I. INTRODUCTION

In a recent paper, Götze and Mayr [1] demonstrated that the mode-coupling theory for the glass transition (MCT) applied to a model of the hard-sphere system (HSS) at relatively high packing fractions yields spectra for the density correlation functions, that display a broad asymmetric peak as well as a sound-like mode at rather high wave vectors. Similar observations have been made in real glass formers and are known as the Boson Peak (BP) and high-frequency sound (HFS), respectively. To investigate these phenomena in detail, a large number of experiments has been performed, using various techniques such as Raman spectroscopy, x-ray spectroscopy, neutron scattering, or molecular-dynamics simulations. For an account of the literature, the reader is referred to the papers cited in [1]. This work also contains a summary of the features signifying both the HFS and the BP.

The mentioned aspects of the full numerical MCT solutions can be understood on the basis of two additional approximations; one being the generalized hydrodynamic (GHD) approximation, the other being the so-called stiff-glass approximation (SGA). Performing these two approximations, one arrives at an equation that, while it still has to be solved numerically, provides physical insight on the origin of the BP- and HFS-like features of the HSS model. Especially the SGA can be understood on physical grounds as a description of phonon scattering from the frozen-in amorphous structure, neglecting two-phonon processes. In [1] a further simplification was carried out. It amounts to dropping the remaining wave-vector dependence of the microscopic frequencies in the GHD-SGA formula. As it leads to an equation that has been discussed earlier as a "schematic" toy model of the MCT, we shall call it the schematic-model description in the following. One obtains an analytically solvable expression that, despite its simplicity, gives a good description of the memory kernel responsible for the BP-like spectra.

The aim of this paper is to drop this last simplification and to consider the SGA equations directly. This way, all of the additional simplifications applied on top of MCT can be investigated independently. We shall also compare with the analytic solution of [1] to understand its range of applicability. The discussion is meant to enlighten the physical mechanism behind the MCT boson peak, since the SGA is connected with a clear-cut physical picture.

The paper is organized as follows: Section II will present a summary of the basic equations and approximations outlined above. In Sec. III, the solutions of the SGA equations with the full q dependence taken into account will be presented. Section IV examines the effect of the GHD and schematic approximations, and Sec. V offers some conclusions.

II. EQUATIONS OF MOTION

A. Mode-Coupling Theory

The mode-coupling theory of the glass transition (MCT) describes the dynamics of a glass-forming liquid in terms of the density correlators $\Phi_q(t) = \langle \varrho_{\vec{q}}^*(t) \varrho_{\vec{q}} \rangle$. Here, $\varrho_{\vec{q}} = \sum_j \exp(i\vec{q}\vec{r}_j)/\sqrt{N}$ are the density fluctuations of wave vector $\vec{q}$, for a system of N particles at density ρ. $\langle \ldots \rangle$ denotes canonical averaging. For amorphous systems, $\Phi_q(t)$ depends on the wave-vector only through its modulus $q = |\vec{q}|$. At short times, one has $\Phi_q(t) = S_q - \frac{1}{2} S_q \Omega_q^2 t^2 + \ldots$, where $S_q = \langle |\varrho_{\vec{q}}|^2 \rangle$ is the static structure factor specifying the equilibrium structure of the system. $\Omega_q^2 = v^2 q^2 / S_q$ are the phonon frequencies. A system of hard spheres shall be considered. The units of time and length are chosen in accordance with [1] such that the thermal velocity $v = 2.5$ and the sphere diameter $d = 1$.

The normalized density correlators $\phi_q(t)$, given by $\Phi_q(t) = S_q \phi_q(t)$, obey the equations of motion obtained via a Mori-Zwanzig projection operator formalism,

$$\ddot{\phi}_q(t) + \Omega_q^2 \phi_q(t) + \Omega_q^2 \int_0^t m_q(t-t') \dot{\phi}_q(t') \, dt' = 0 \,. \quad (1a)$$

Here $m_q(t)$ is the memory kernel, a correlation function of fluctuating forces. If one introduces Fourier-Laplace transformed quantities with the convention $\phi_q(z) =$

$i \int_0^\infty \exp(izt)\phi_q(t)dt$, Eq. (1a) is equivalent to

$$\chi_q(z)/\chi_q^0 = -\Omega_q^2/\left[z^2 - \Omega_q^2 + \Omega_q^2 z m_q(z)\right] , \qquad (1b)$$

where the fluctuation dissipation theorem has been used to connect $\phi_q(z)$ to the dynamical susceptibility $\chi_q(z)$: $\chi_q(z)/\chi_q^0 = z\phi_q(z) + 1$, with χ_q^0 denoting the isothermal compressibility.

Within MCT, the memory kernel $m_q(t)$ is written as the sum of a regular contribution and a so-called mode-coupling contribution, the latter describing the slow dynamics important close to the glass transition. For details, the reader is referred to the original publications [2, 3] and standard literature [4]. One gets for $m_q(t)$ a quadratic functional in $\phi(t)$, $m_q^{\mathrm{MCT}}(t) = \mathcal{F}_q[\phi]$,

$$m_q^{\mathrm{MCT}}(t) = \int_{\vec{p}=\vec{q}-\vec{k}} \frac{d^3k}{(2\pi)^3} V(\vec{q}\vec{k}\vec{p})\phi_k(t)\phi_p(t) , \qquad (2a)$$

with coupling coefficients given by the equilibrium structure of the system,

$$V(\vec{q}\vec{k}\vec{p}) = \rho S_q S_k S_p[(\vec{q}\vec{k})c_k + (\vec{q}\vec{p})c_p]^2/(2q^4) . \qquad (2b)$$

Here c_q denotes the Ornstein-Zernike direct correlation function, connected to the static structure factor by $S_q = 1/(1 - \varrho c_q)$. If one introduces a wave-vector grid and approximates the integral as a Riemann sum, the mode-coupling functional can be written as $\mathcal{F}_q[f] = \sum_{kp} V_{qkp}f_k f_p$, where k and p run over the set of all grid points. The coefficients V_{qkp} are trivially related to the $V(\vec{q}\vec{k}\vec{p})$.

For the discussion of the MCT dynamics in the boson-peak region, Götze and Mayr [1] chose a model of the hard-sphere system, given by evaluating S_q in the Percus-Yevick approximation, introducing a grid of $M = 300$ wave vectors q with a cutoff of $q^* = 40$, and by neglecting the regular part of the memory kernel. The dependence of the solutions on these approximations will have to be investigated seperately. For the structure factor used, a cutoff dependence of the solutions cannot be neglected, as was already mentioned in [1], and one is lead to the conclusion that the model described here is one of a soft-core fluid rather than true hard spheres. Even more so, the influence of the regular term is unclear at present. Recent calculations indicate that, at least in the white-noise approximation based on a generalized Enskog theory, the regular damping might be so large as to render the BP part of the spectrum nonexistent for a true hard-sphere system [5]. The question, however, remains unanswered still for regular potentials. Nevertheless, since the concern of this paper is a comparison with the results presented in [1], we shall choose all numerical parameters the same. Equations (1) and (2) are closed then, and since S_q for the hard-sphere system does not depend on temperature, the only control parameter is the density ρ, which shall be written as the packing fraction $\varphi = \pi\rho/6$.

B. Stiff-Glass Approximation

The starting point for a theoretical understanding of the MCT high-frequency dynamics is a reformulation of the equations of motion, Eqs. (1), within the glass state. One introduces new correlators $\hat{\phi}_q(t)$ that only deal with the decay relative to the frozen structure given by the nonergodicity parameter f_q, $\phi_q(t) = f_q + (1 - f_q)\hat{\phi}_q(t)$. Equations (1) are covariant in the sense that the same equations hold for the new variables,

$$\chi_q(z)/\hat{\chi}_q^0 = -\hat{\Omega}_q^2/\left[z^2 - \hat{\Omega}_q^2(1 - z\hat{m}(z))\right] , \qquad (3)$$

provided one replaces the static susceptibility by $\hat{\chi}_q^0 = \chi_q^0(1 - f_q)$, the frequencies Ω_q^2 by

$$\hat{\Omega}_q^2 = \Omega_q^2/(1 - f_q) , \qquad (4)$$

and the memory kernel by

$$\hat{m}_q(t) = \hat{\mathcal{F}}_q^{(1)}[\hat{\phi}] = \hat{\mathcal{F}}_q^{(1)}[\hat{\phi}] + \hat{\mathcal{F}}_q^{(2)}[\hat{\phi}] , \qquad (5a)$$

$$\hat{\mathcal{F}}_q^{(1)}[\hat{f}] = \sum_k \hat{V}_{qk}\hat{f}_k , \qquad (5b)$$

$$\hat{\mathcal{F}}_q^{(2)}[\hat{f}] = \sum_{kp} \hat{V}_{qkp}\hat{f}_k\hat{f}_p , \qquad (5c)$$

with new coupling coefficients given by

$$\hat{V}_{qk} = 2(1 - f_q)\sum_p V_{qkp}f_p(1 - f_k) , \qquad (6a)$$

$$\hat{V}_{qkp} = (1 - f_q)V_{qkp}(1 - f_k)(1 - f_p) . \qquad (6b)$$

The new variables $\hat{\phi}_q(t)$ and $\hat{m}_q(t)$ have the properties that their long-time limits vanish, thus the low-frequency limits of their Laplace transforms are regular.

To study BP phenomena, the limit of high packing fraction is of interest. There the original coupling coefficients become large, formally written $V_{qkp} = \mathcal{O}(1/\eta)$ with some small parameter η. The virtue of the covariant transformation now is that it implies $1 - f_q = \mathcal{O}(\eta)$, and thus

$$\hat{V}_{qk} = \mathcal{O}(\eta) , \qquad \hat{V}_{qkp} = \mathcal{O}(\eta^2) , \qquad (7)$$

i.e. the new coupling coefficients become small. This suggests to drop the second-order contribution to the memory kernel $\hat{m}_q(t)$, such defining the stiff-glass approximation (SGA), cf. Eq. (14) of [1]:

$$\hat{\phi}_q^{(1)}(z) = -1/\left[z - \hat{\Omega}_q^2/\left[z + \hat{\Omega}_q^2\hat{m}_q^{(1)}(z)\right]\right] , \qquad (8a)$$

$$\hat{m}_q^{(1)}(z) = \sum_k \hat{V}_{qk}\hat{\phi}_k^{(1)}(z) . \qquad (8b)$$

Equations similar to Eq. (8) were derived in a different context by other authors. Let us, for example, rewrite these equations in a notation closer to the conventions of

field theory. The dynamical susceptibility can be rewritten for positive frequencies $z = \omega^2$, $\omega > 0$, into a propagator $G(q,\omega) = -\hat{\chi}_q^{(1)}(\sqrt{z})/(\hat{\chi}_q \hat{\Omega}_q^2)$, depending on the bare dispersion relation $\epsilon(q) = \hat{\Omega}_q^2(1 + \sum_k \hat{V}_{qk})$, and on the complex self energy $\Sigma(p,\omega)$, to give

$$G(q,\omega) = \frac{1}{\omega - \epsilon(q) - \Sigma(q,\omega)} \qquad (9a)$$

$$\Sigma(q,\omega) = \int dk\, \tilde{V}_{qk} G(k,\omega)\,, \qquad (9b)$$

where $\tilde{V}_{qk} = \hat{\Omega}_q^2 \hat{V}_{qk} \hat{\Omega}_k^2$ are positive coupling constants. This is equivalent to the equations discussed by Martín-Mayor *et al.* [6] and Grigera *et al.* [7] in connection with Euclidean random matrix theory, cf. Eqs. (13) and (17) of the latter paper, where, however, the vertices $\tilde{V}_{qk}$ are different. Equations (9) can be viewed as a special case of the Dyson equation [8].

Equations (8) still have to be solved numerically. Thus, Götze and Mayr [1] proposed two additional simplifications, the first of which is the Generalized Hydrodynamic (GHD) description. One replaces the memory kernel $\hat{m}_q^{(1)}(z)$ by its ($q \to 0$) limit, $K(z) = \hat{m}_{q=0}^{(1)}(z)$. If one is only interested in a description of sound modes at small q, one could also replace the frequencies by their leading-order contributions, $\hat{\Omega}_q = v_\infty q + \mathcal{O}(q^2)$, with the high-frequency sound velocity $v_\infty = v/\sqrt{(1-f_0)S_0}$. In the following, we will only discuss the GHD-SGA obtained by keeping the full q-dependence of $\hat{\Omega}_q$,

$$\hat{\chi}_q^{\text{GHD}}(z)/\hat{\chi}_q = -\hat{\Omega}_q^2 / \left[z^2 - \hat{\Omega}_q^2(1 - zK(z)) \right]\,. \qquad (10)$$

A further simplification was obtained in [1] by replacing $\hat{\Omega}_q$ with some q-independent averaged value $\tilde{\Omega}$. This was motivated by the observation that in the range around the first diffraction peak in the structure factor, a q range known to constitute the dominant contribution to the mode-coupling kernel [2], the variation of the renormalized values $\hat{\Omega}_q$ with q is suppressed relative to that of Ω_q. As a result, one arrives at

$$\tilde{\phi}(z) = -1/\left[z - \tilde{\Omega}^2/\left[z + \tilde{\Omega}^2 \tilde{K}(z) \right] \right]\,, \qquad (11a)$$

$$\tilde{K}(z) = w_1 \tilde{\phi}(z)\,, \qquad (11b)$$

with $w_1 = \int dk\, \hat{V}_{0k}$. The set of Eqs. (11a,11b) constitutes a well-known schematic model of MCT discussed earlier [4, 9, 10], the so-called F_1 model. It can be solved trivially for either $\tilde{\phi}(z)$ or $\tilde{K}(z)$. With the notation $z = \omega + i0$ we get

$$\tilde{K}(\omega) \approx \left[\omega_+ \omega_- - \tilde{\omega}^2 + \sqrt{\tilde{\omega}^2 - \omega_-^2}\sqrt{\tilde{\omega}^2 - \omega_+^2} \right]/(2\omega)\,, \qquad (12)$$

with $\omega_\pm = 1 \pm \sqrt{w_1}$, and $\tilde{\omega}^2 = \omega^2/\tilde{\Omega}^2$. The "semi-ellipse" spectrum $\tilde{K}''(\omega)$ thus obtained was demonstrated in [1]

to have striking similarities to the spectra of the full MCT solutions in the BP regime at $\varphi = 0.6$.

Eq. (12) implies a "gap" in the kernel spectrum for $0 < \omega < \omega_-$. The full solutions show a pseudo-gap for frequencies below the BP frequency resembling this finding. The smearing out of the gap due to two-phonon processes can be understood on the basis of the schematic model by including these processes in a perturbative manner, which amounts to replacing $\tilde{K}(\omega)$ in Eq. (11a) with $\tilde{K}^{(2)}(\omega) = \tilde{K}(\omega) + K^{(2)}(\omega)$, where the latter term reads [1]

$$K^{(2)}(\omega) = \frac{1}{\pi}\frac{w_2}{w_1^2} \int \tilde{K}(\omega - \omega')\tilde{K}''(\omega')\, d\omega'\,, \qquad (13)$$

with the integrated second-order coupling coefficient $w_2 = \int dk\, \hat{V}_{0kk}$. $\tilde{K}^{(2)}(\omega)$ is then still given by Eq. (12), but one has to set $\tilde{\omega}^2 = \omega^2/\tilde{\Omega}^2 + K^{(2)}(\omega)$. Analytic solvability can be regained by evaluating this in the ($\omega \to 0$) limit, $K^{(2)}(\omega \to 0) = i\tau$,

$$\tau = \frac{w_2}{\sqrt{w_1}}\frac{8}{3\pi\tilde{\Omega}}\,. \qquad (14)$$

Since arriving at Eq. (12) involved three subsequent approximations which, in principle, could be applied independently from one another, it seems worthwhile to discuss the effects of each approximation by itself. Especially going over to the schematic model description of the memory kernel as a last step is, in contrast to the GHD-SGA, uncontrolled in the sense that its derivation is not based on a well-defined mathematical procedure.

The GHD approximation was shown in [1] to be of very good quality, provided on does apply it to the transformed memory kernel $\hat{m}_q(z)$. In other words, keeping the full q-dependence of the nonergodicity parameters f_q is of vital importance for a description of the BP and HFS spectra. It can thus be expected to be of similar quality when applied together with the SGA.

While not leading to analytically solvable expressions, the SGA alone, Eqs. (8), has a clear-cut physical meaning: The first-order contribution to the memory kernel can be interpreted as an elastic scattering of phonons due to the frozen disorder in the glass, a mechanism thought to be dominant over two-phonon decay processes, which are represented by the second-order term and therefore ignored in the SGA. It should be noted, however, that this does not correspond to a harmonic approximation.

III. SOLUTION OF THE SGA EQUATIONS

To obtain numerical solutions of Eqs. (8), an algorithm adapted from the one used in [1] was employed. It solves the initial-value problem for the coupled integro-differential equations corresponding to Eqs. (8) in the time domain. Regarding the stability of this method, proofs are available [11], which apply to the SGA as a
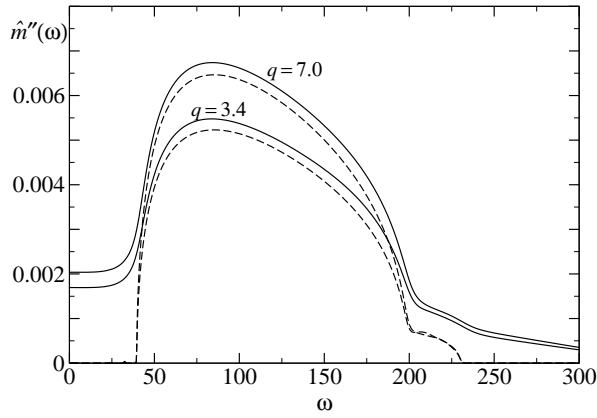
FIG. 1: Transformed memory-kernel spectra $\hat{m}_q''(\omega)$ of the full-MCT solutions for the HSS model, Eq. (3), for wave vectors $q = 3.4$, and $q = 7.0$, at packing fraction $\varphi = 0.6$ (solid lines). The dashed lines show the corresponding spectra obtained within the stiff-glass approximation (SGA), Eq. (8).

special case. Here it merely is important that the mode-coupling vertices $\hat{V}_{qk}$ are positive. The solutions were Fourier transformed to give the spectra $\phi_q''(\omega)$ and $m_q''(\omega)$.

Let us start the discussion by a comparison of the memory kernel spectra $\hat{m}_q''(\omega)$, obtained from the solution of the full MCT equations, Eq. (3), and of the SGA equations, Eq. (8). Figure 1 shows such a comparison for packing fraction $\varphi = 0.6$. One notes a dominant broad and asymmetric peak responsible for the BP features of the correlator spectra [1]. The SGA solutions still recover the shape of that peak reasonably well; an observation together with its form being reminiscent of the semi-ellipse known from the schematic model further justifying the analogy put forward by the schematic model description. At frequencies $\omega \lesssim 40$, a pseudo-gap can be seen. As discussed in [1], the SGA spectrum is not exactly zero within this gap; rather one obtains Rayleigh's law, $\hat{m}_q^{(1)''}(\omega) = R_q \omega^2 + \mathcal{O}(\omega^4)$. The prefactor of the Rayleigh contribution is, however, so small that it is invisible in the plot shown. Comparing with the full MCT solution, one clearly notes the filling of the gap due to the two-phonon modes.

On the high-frequency wing, the spectra obtained from the full solutions show a nontrivial decay to zero, including, for larger q vectors, a second small peak at frequencies $200 \lesssim \omega \lesssim 250$. Interestingly enough, this peak is also reproduced by the SGA memory kernels.

Since the SGA reproduces the memory kernel of the full MCT solutions resonably well in the frequency range of importance for the discussion of BP-like phenomena, it comes as no surprise that it also gives a basically correct description of the density correlator spectra $\Phi_q''(\omega)$. Figure 2 compares these spectra to those of the full MCT equations. The BP spectra are, with some quantiative differences, largely correct within the SGA, and the same holds for the HFS modes for those q vectors, where the sound damping is dominated by the BP background. At
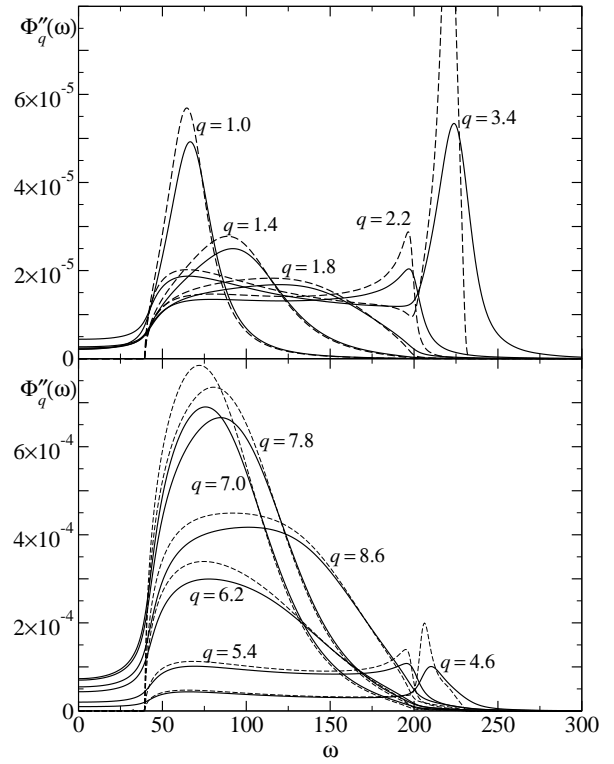

FIG. 2: Dynamical structure factor $S(q, \omega) = S_q \phi_q''(\omega)$ for different wave vector q as labeled at packing fraction $\varphi = 0.6$. The solid lines show the solutions obtained from the full equations, Eqs. (1). The dashed lines are the corresponding SGA spectra, Eqs. (8).

$q \sim q_{\mathrm{D}}$, where $q_{\mathrm{D}} \approx 4$ is the Debye frequency [1], the SGA sound-mode damping clearly is too small. This failure is to be expected from the above discussion of the memory kernel, since in this case the sound resonance maximum occurs at frequencies above the BP spectrum, where the SGA memory kernel spectrum is too small. Similarly, the pseudo-gap at low frequencies and the rapid decay at large ω within the SGA are a result of the same features of the memory kernel spectra.

The SGA is based on the two-mode contributions of order $\mathcal{O}(\eta^2)$ being neglegible in comparison to one-mode contributions of order $\mathcal{O}(\eta)$. The quality of this approximation is expected to decrease with lowering the packing fraction, since η increases with decreasing φ. Figures 3 and 4 repeat the comparison made in Fig. 2, now for packing fractions $\varphi = 0.5676$ and $\varphi = 0.54$, respectively. One can identify the increasing intensity for low frequencies, eventually becoming so strong as to dominate over the BP background for $\varphi = 0.54$. Nevertheless, the SGA gives the qualitatively correct picture even for $\varphi = 0.54$ at frequencies $\omega \gtrsim 25$, the number depending somewhat on the wave vector. One also notices the shift of both the sound resonance and the BP maximum to lower frequencies as the packing fraction decreases. This further demonstrates two features typical for the BP and the HFS [1].
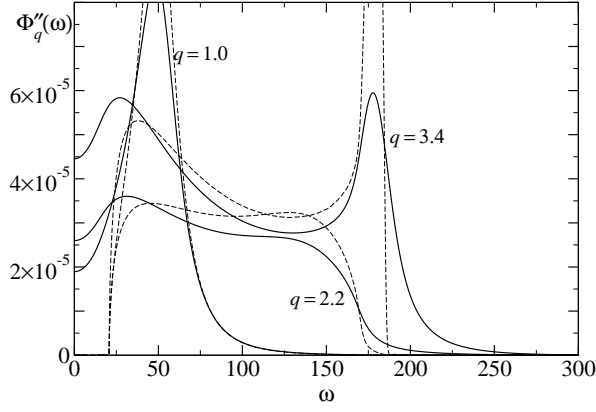
FIG. 3: Comparison of full MCT and SGA for spectra $\Phi_q''(\omega)$ as in Fig. 2, but for $\varphi = 0.5676$, and wave vectors $q = 1.0$, 2.2, and 3.4. Other q were left out to avoid overcrowding the figure.
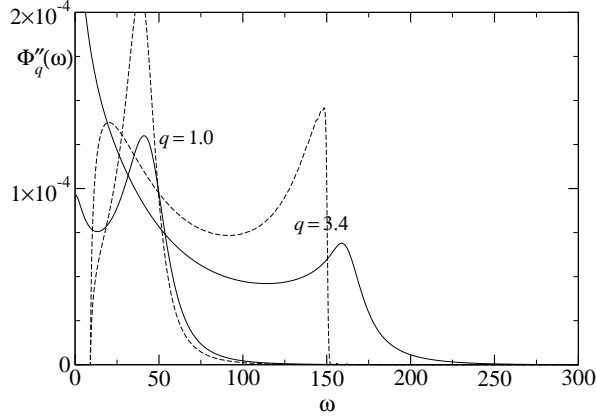

FIG. 4: Comparison of full MCT and SGA for spectra $\Phi_q''(\omega)$ as in Fig. 2, but for $\varphi = 0.54$, and wave vectors $q = 1.0$ and $q = 3.4$.

One notes that for $\varphi = 0.54$ and $\varphi = 0.5676$ the true HFS maximum positions are higher than those read off the SGA solutions, especially for q vectors where the SGA significantly underestimates the damping. This effect is also known as level repulsion. For a discussion of the effects of the SGA on the HFS modes, Figs. 5 and 6 show the maximum positions of the spectra $\phi_q''(\omega)$ and the resonance widths versus wave vector q for different packing fractions. Two maximum positions are noted whenever the BP background and the HFS mode could be identified as distinct, separated by a spectral minimum. The full widths at half maximum (FWHM) were obtained by marking the lowest and the highest frequency where the correlator spectrum reaches half the value of its global maximum.

For the HFS maxima as well as the BP maxima at $\varphi = 0.6$, Fig. 5, good agreement between the full solutions, reproduced from [1], and the SGA solutions is found. This even holds in the low-q regime, where only a damped sound mode can be seen in the spectra. Here
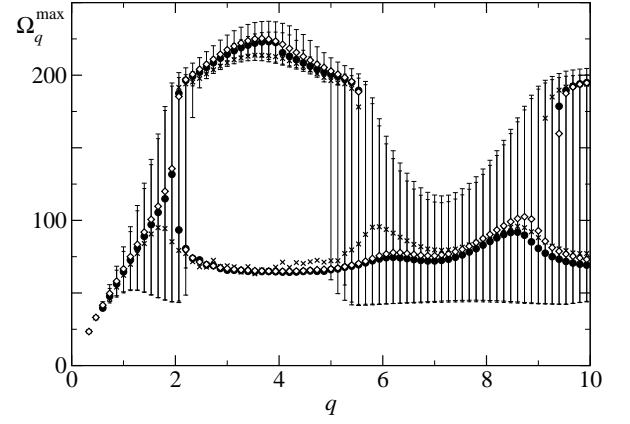

FIG. 5: Maximum positions of the density-correlator spectra $\phi_q''(\omega)$ obtained from the full MCT solutions at $\varphi = 0.6$ versus wave vector q (open diamonds). Two symbols are drawn where two distinct maxima (separated by a minimum) could be identified. Filled circles indicate the maximum positions obtained within the SGA, Eq. (8), while crosses correspond to the results of the SGA-GHD, Eq. (10). The bars indicate the full widths at half maximum (FWHM) as described in the text. The smaller bars are FWHM of the SGA solutions, FWHM data for the SGA-GHD is left out to enhance readability.

the shift in the maximum position due to damping is still small, such that an underestimation of the damping by the SGA does not necessarily lead to a wrong description of the position. The agreement of the FWHM values also is good, with the reservation that the SGA values are too small in general. The lower frequency for which the spectrum reaches half the maximum intensity is described better than the higher one within the SGA, since here the pseudo-gap marks the dominant rise in the spectrum.

Comparing the maximum positions and FWHM at $\varphi = 0.5676$, one notes that for the BP maximum, the agreement between full MCT and SGA still is very good. Expectedly, the description of the FWHM is worse, mostly due to the appearance of the pseudo-gap and due to the underestimation of the sound-mode damping around q_D.

The sound damping in the regime of the HFS is illuminated in more detail in Fig. 7. Here, full width at half maximum values Γ_q obtained from the full solutions of Eq. (3) and from within the SGA, Eq. (8), are compared for the two packing fractions $\varphi = 0.6$ and $\varphi = 0.5676$. For $q \leq 0.6$ (0.467) at $\varphi = 0.6$ (0.5676), the SGA line widths could not be determined reliably. This reflects a limitation of the numerical procedure used, which is not adequate for very weakly damped oscillations, as occuring within the SGA. Nevertheless, the errors introduced by the numerical algorithm for low q do not significantly affect the accuracy of the solutions for larger q, since the small-q contribution to the memory kernel is neglegible [2].
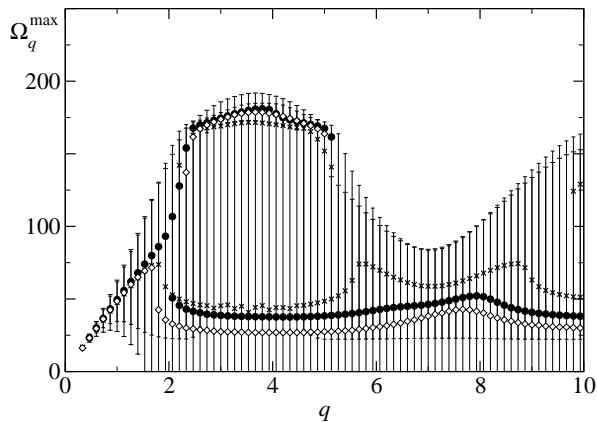
The dashed lines in Fig. 7 show the low-q asymp-

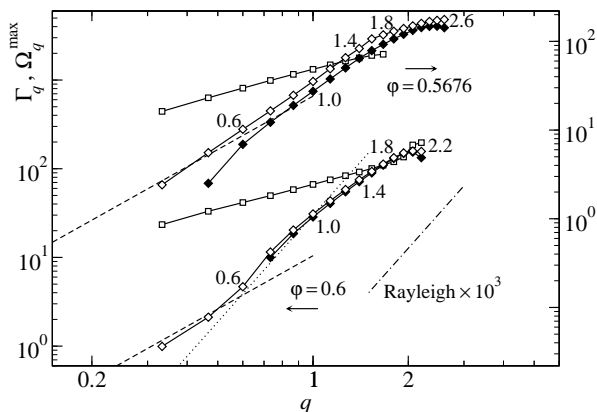FIG. 6: Same as Fig. 5, but for packing fraction $\varphi = 0.5676$.

FIG. 7: Double-logarithmic plot of linewidths Γ_q (diamonds) and maximum positions $\Omega_q^{\max}$ (squares) of the density-correlator spectra versus wave vector q in the high-frequency-sound regime. The lower set of data corresponds to packing fraction $\varphi = 0.6$ (labels on left axis). The upper set shows the same data for $\varphi = 0.5676$ (labels on right axis). Open symbols are values determined from the solutions of the full MCT, filled symbols demonstrate the SGA solutions. The dashed lines correspond to the low-q asymptote, $\Gamma_q = q^2\gamma$ (see text). The dotted line corresponds to a q^4 power law, while the dot-dashed line demonstrates the Rayleigh contribution for $\varphi = 0.6$, multiplied by a factor of 10^3.

tote for the full MCT solutions, $\Gamma_q = q^2\gamma$, with $\gamma = v_\infty^2 \hat{m}_{q=0}''(\omega \to 0)$. One notices an enhancement above the asymptotic q^2 law for $q \gtrsim 0.6$. At around $q = 1.4$, the resonance width becomes of the same order of magnitude as its position, $\Omega_q^{\max}$, and thus a Ioffe-Regel limit is reached. Above this point, the line shapes differ significantly from a Lorentzian and hybridization with the BP modes becomes important. For $\varphi = 0.5676$, the maximum positions $\Omega_q^{\max}$ are smaller than for $\varphi = 0.6$, while the damping Γ_q changes only weakly in the regime of the enhancement over the asymptotic law, a behavior also found in experiment [12, 13]. Only for very small q vectors, $q \lesssim 0.6$, one notices in the full MCT solutions the expected behavior of Γ_q.

In the q range from $q \approx 0.6$ to $q \approx 1.4$, the data for $\varphi = 0.6$ can be approximately described by some power law, with its exponent being close to 4. To demonstrate this, the dotted line was included in Fig. 7, representing a q^4 law. While in some investigations, no indication of such a q^4 law was found [14], it has been argued that this is behaviour is connected to Rayleigh's law [15]. In the present case, however, the approximate q^4 power law is not an indication for Rayleigh scattering. As already noted in [1], the Rayleigh contribution R_q is much lower. It is included in Fig. 7 as the dot-dashed line. Note that a magnification by a factor of 1000 was necessary to make this contribution visible in the plot. Thus one concludes, that the q^4 law for the high-frequency sound is a mere numerical coincidence. The possible appearance of a pseudo-power law for the HFS line width can be seen even more clearly for $\varphi = 0.5676$, where an exponent between 2 and 4 would be obtained.

Fig. 7 again demonstrates the validity of the SGA. At and below $q \sim 0.6$, deviations are to be expected, since the SGA line widths do not obey the asymptotic q^2 law. Rather one expects the SGA damping for $q \to 0$ to be given by Rayleigh's law noted above. Despite this fact, the overall description of Γ_q by the SGA is quite good.

IV. EFFECT OF ADDITIONAL APPROXIMATIONS

Having discussed the quality of the SGA in comparison to a full MCT solution, we shall now turn to a discussion of the additional simplifications outlined in the introduction. Since the q dependence of the memory kernel spectra is weak, cf. Fig. 1, one is lead to the combination of both the GHD approximation and the SGA. Figure 8 shows a comparison of thus obtained density-correlator spectra with selected full-MCT and SGA spectra reproduced from Fig. 2. Indeed, good agreement is found for the experimentally relevant q-vector range at $q \lesssim q_{\mathrm{D}}$.

The GHD-SGA solution fails to produce reasonable sound modes for wave vectors where the position of the sound maximum is at about the upper cutoff for the BP memory kernel. This is due to the sensitivity of the shape of the memory kernel in this frequency region. As noted in connection with Fig. 1, the SGA still reproduces the nontrivial second peak in $m_q''(\omega)$ also seen in the full MCT solutions. Since this peak only evolves for higher q vectors, the GHD approximation obviously misses this feature, resulting in only weakly damped sound modes there. Still, the GHD-SGA combination is valuable for a discussion of BP-like spectra and the hybridization effects occuring between HFS modes and the BP spectra. Note that the maximum positions obtained from the GHD-SGA description show a qualitatively correct behavior. This can be seen from Figs. 5 and 6. Within the hybridization regime, the FWHM values (not shown in the figures) also are almost quantitatively correct.

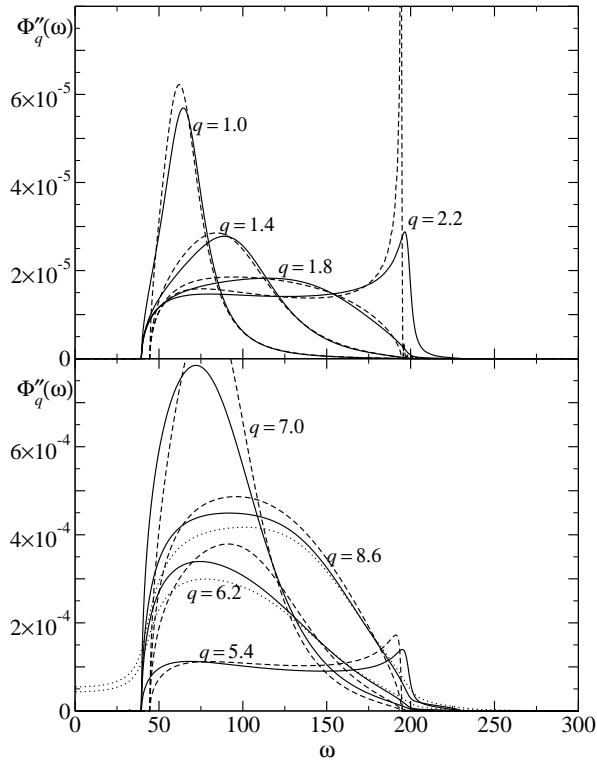A comparison between the full solutions and those ob-

FIG. 8: Spectra for $\varphi = 0.6$ and q vectors as labeled obtained within the SGA (solid lines, reproduced from Fig. 2). Dashed lines show the corresponding spectra obtained within the GHD description in addition to the SGA. The dotted lines show examples for the full solutions (taken from Fig. 2).

tained by applying the GHD only, still including two-phonon modes, was given in Fig. 6 of [1]. There it can be seen that the GHD approximation is, for $q \lesssim q_D$, at least as good as the SGA, at the expense of still requiring the computation of a nonlinear memory kernel. Only the combination of both SGA and GHD seems to be too crude to deal with high-frequency sound modes for all wave vectors. For higher q vectors, the GHD-only approximation of [1] and consequently also the GHD-SGA description somewhat miss the shape of the BP background spectra, as is evident from the lower panel of Fig. 8. On the other hand, the SGA discussed here regains better quality for those q-vector regions where the HFS mode again shows hybridization with the BP-like spectrum. This shows that in this region, one-mode contributions from higher q vectors are important to fully explain the shape of the BP phenomena.

As a last step, one can also compare the memory kernel spectra resulting from the SGA in the $q \to 0$ limit with the schematic model description proposed by Götze and Mayr, Eqs. (11). Fig. 13 of [1] presented a comparison at $\varphi = 0.6$ between the schematic model semi-ellipse and the full-MCT kernel spectrum at $q = 0$. Let us extend the discussion by adding the corresponding SGA spectrum. This is done in Fig. 9, while Figs. 10 and 11 carry the same comparison to lower packing fractions, $\varphi = 0.5676$
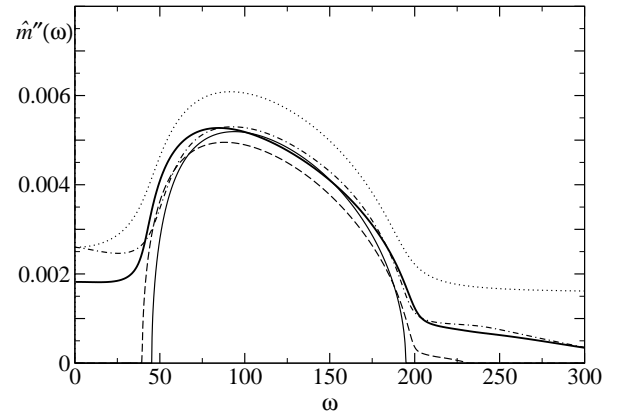

FIG. 9: Memory kernel spectrum for $\varphi = 0.6$ and $q = 0$. The spectrum $\hat{m}''_{q=0}(\omega)$ obtained from the full MCT equations, Eq. (3), is shown as the thick solid line. The dashed line shows the SGA result. The schematic-model descriptions shown in Fig. 13 of [1] are also reproduced: the thin solid line is the semi-ellipse obtained from Eq. (12), the dotted line is the spectrum with τ evaluated from Eq. (14), see text for details. The dot-dashed line represents the result for the schematic model with a frequency-dependent second-order correction, Eq. (13), included.
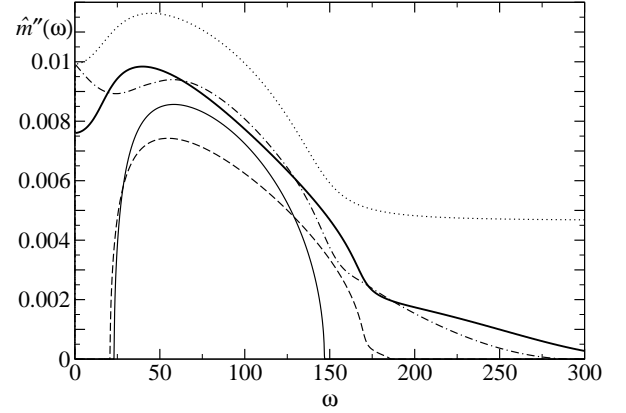

FIG. 10: As Fig. 9, but for $\varphi = 0.5676$.

and $\varphi = 0.54$, respectively. The averaged frequency was chosen to be $\tilde{\Omega} = 120$ for $\varphi = 0.6$, in accordance with [1], and $\tilde{\Omega} = 85$ (60) for $\varphi = 0.5676$ (0.54). One could improve on these values, but this would not give further physical insight, nor would it significantly alter the results discussed below.

The success of the semi-ellipse description at $\varphi = 0.6$ is based largely on the fact, that in the relevant q range, the variations of $\hat{\Omega}_q$ are suppressed as η becomes small. For lower packing fractions, the relative variations in $\hat{\Omega}_q$ are larger. Together with the increasing two-mode contributions, this leads to stronger deviations of the full-MCT spectra from the schematic semi-ellipse form.

As explained above, the two-mode contributions can within the schematic description be accounted for approximately by including a frequency-independent damp-
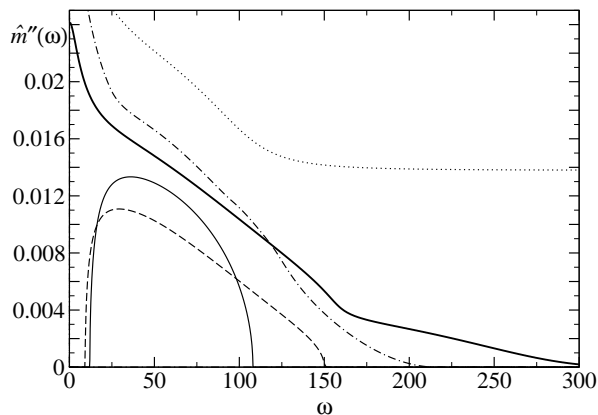
FIG. 11: As Fig. 9, but for $\varphi = 0.54$.

ing term, Eq. (14). While this procedure works well for $\varphi = 0.6$, it does not lead to an satisfactory result at the two lower packing fractions investigated here, cf. Figs. 10 and 11. One needs to go beyond the white-noise approximation and include a frequency-dependent term, Eq. (13). Then the spectra are described fairly, but the advantage of analytic solvability is lost.

However, the SGA solutions include no second-order contributions and thus should be compared to the pure semi-ellipse of the schematic description. It is remarkable that the SGA on the other hand catches the nontrivial shape of the BP-like contribution to the memory kernel spectrum qualitatively correct even at lower packing fractions, albeit with an overall too low intensity. The "tail" of the spectrum as well as the evolving central peak is missing in the SGA solution due to the well-understood occurence of the pseudo-gap.

V. CONCLUSIONS

The stiff-glass approximation (SGA) to the mode-coupling theory of the glass transition (MCT) was dis-

cussed and shown to provide a good description of the spectra in the boson-peak regime. It holds valid even for packing fractions lower than $\varphi = 0.6$, where the analytical formula of Götze and Mayr [1], Eq. (12), cannot describe the memory kernel any longer. This failure of Eq. (12) is due to increasing variations with q in the phonon dispersion $\hat{\Omega}_q$, which in the schematic model is neglected. The shape of the SGA memory kernel shows more structure than a simple semi-ellipse form. This leads to a substantially correct description of high-frequency sound and sound damping in this approximation.

Even the combination of the SGA with the generalized hydrodynamic description (GHD) gives reasonable results for the memory kernels as well as for the density correlators, for q vectors where the damping of the sound mode is dominated by contributions from the BP-like memory kernel. Outside this window, one gets weakly damped sound waves, an artifact introduced in the intermediate q range mainly by the GHD, not the SGA. Nevertheless, the GHD-SGA gives a basically correct description of the BP spectra. This finding further corroborates the explanation of the HFS as a result of the BP spectra.

As a side effect, it was demonstrated, that equations of the form of Eqs. (8) can be solved relatively easy in the time domain. At first glance, this seems paradox, since in Eq. (8), both q and frequency z only appear as parameters, while in the time domain one has to solve a convolution integral.

[1] W. Götze and M. R. Mayr, Phys. Rev. E **61**, 587 (2000).
[2] U. Bengtzelius, W. Götze, and A. Sjölander, J. Phys. C **17**, 5915 (1984).
[3] E. Leutheusser, Phys. Rev. A **29**, 2765 (1984).
[4] W. Götze, in *Liquids, Freezing and Glass Transition* (North Holland, Amsterdam, 1991), vol. Session LI (1989) of *Les Houches Summer Schools of Theoretical Physics*, pp. 287–503.
[5] M. Sperl, *private communication* (2001).
[6] V. Martín-Mayor, M. Mézard, G. Parisi, and P. Verrocchio, J. Chem. Phys. **114**, 8068 (2001).
[7] T. S. Grigera, V. Martín-Mayor, G. Parisi, and P. Verocchio, *Vibrational spectra in glasses* (2001), cond-mat/0104433.
[8] E. N. Economou, *Green's Functions in Quantum Physics*, vol. 7 of *Springer Series in Solid-State Sciences* (Springer, Berlin, 1983), 2nd ed.
[9] W. Götze and L. Sjögren, J. Phys. C **17**, 5759 (1984).
[10] R. L. Jacobs, J. Phys. C **19**, L119 (1986).
[11] W. Götze and L. Sjögren, J. Math. Analysis and Appl. **195**, 230 (1995).
[12] C. Masciovecchio, G. Ruocco, F. Sette, P. Benassi, A. Cunsolo, M. Krisch, V. Mazzacurati, A. Mermet, G. Monaco, and R. Verbeni, Phys. Rev. B **55**, 8049 (1997).
[13] G. Monaco, C. Masciovecchio, G. Ruocco, and F. Sette, Phys. Rev. Lett. **80**, 2161 (1998).
[14] G. Ruocco, F. Sette, R. D. Leonardo, G. Monaco, M. Sampoli, T. Scopigno, and G. Viliani, Phys. Rev. Lett. **84**, 5788 (2000).

[15] E. Rat, M. Foret, E. Courtens, R. Vacher, and M. Arai,
Phys. Rev. Lett. **83**, 1355 (1999).